Impact of Ba to Si deposition rate ratios during molecular beam epitaxy on carrier concentration and spectral response of BaSi$_2$ epitaxial films

Ryota Takabe, Tianguo Deng, Komomo Kodama, Yudai Yamashita, Takuma Sato, Kaoru Toko, and Takashi Suemasu

---

Articles you may be interested in

Low temperature synthesis of highly oriented p-type Si$_{1-x}$Ge$_x$ (x: 0–1) on an insulator by Al-induced layer exchange
Journal of Applied Physics **122**, 155305 (2017); 10.1063/1.4996373

Ab initio molecular dynamics simulations of AlN responding to low energy particle radiation
Journal of Applied Physics **123**, 045904 (2018); 10.1063/1.5009750

Silicon photoresistive sensors with improved performance
Journal of Applied Physics **123**, 044505 (2018); 10.1063/1.5006819

LPCVD homoepitaxy of Si doped β-Ga$_2$O$_3$ thin films on (010) and (001) substrates
Applied Physics Letters **112**, 052104 (2018); 10.1063/1.5017616

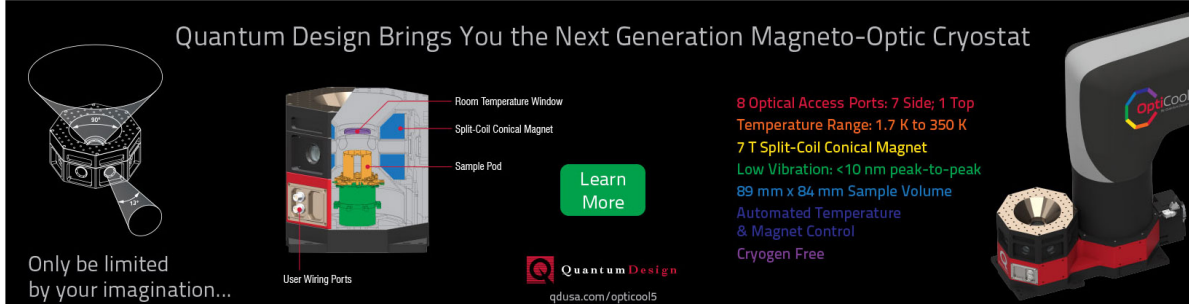Guest Editorial: The dawn of gallium oxide microelectronics
Applied Physics Letters **112**, 060401 (2018); 10.1063/1.5017845

High n-type Sb dopant activation in Ge-rich poly-Ge$_{1-x}$Sn$_x$ layers on SiO$_2$ using pulsed laser annealing in flowing water
Applied Physics Letters **112**, 062104 (2018); 10.1063/1.4997369

CrossMark
click for updates

Impact of Ba to Si deposition rate ratios during molecular beam epitaxy on carrier concentration and spectral response of BaSi$_2$ epitaxial films

Ryota Takabe, Tianguo Deng, Komomo Kodama, Yudai Yamashita, Takuma Sato, Kaoru Toko, and Takashi Suemasu
Institute of Applied Physics, University of Tsukuba, Tsukuba, Ibaraki 305-8573, Japan

Undoped 0.5-μm-thick BaSi$_2$ epitaxial films were grown on Si(111) substrates with various ratios of the Ba deposition rate to the Si deposition rate (R_{Ba}/R_{Si}) ranging from 1.0 to 5.1, and their electrical and optical properties were characterized. The photoresponse spectra drastically changed as a function of R_{Ba}/R_{Si}, and the quantum efficiency reached a maximum at $R_{Ba}/R_{Si} = 2.2$. Hall measurements and capacitance versus voltage measurements revealed that the electron concentration drastically decreased as R_{Ba}/R_{Si} approached 2.2, and the BaSi$_2$ films with R_{Ba}/R_{Si} = 2.0, 2.2, and 2.6 exhibited p-type conductivity. The lowest hole concentration of approximately 1×10^{15} cm^{-3} was obtained for the BaSi$_2$ grown with $R_{Ba}/R_{Si} = 2.2$, which is the lowest value ever reported. First-principles calculations suggest that Si vacancies give rise to localized states within the bandgap of BaSi$_2$ and therefore degrade the minority-carrier properties. *Published by AIP Publishing.*
https://doi.org/10.1063/1.4994850

I. INTRODUCTION

Recently, Kaneka Corporation has achieved the conversion efficiency (η) exceeding 26% in a heterojunction back-contact-type crystalline silicon (c-Si) solar cell. This broke the old record for η of 25.6% and brings η closer to the performance limit determined by the Si bandgap E_g^{Si} of 1.1 eV.[1,2] To develop improvements in η with lower cost, many researchers have paid much attention to Cu(In,Ga)(S,Se)$_2$, CdTe, and perovskite solar cells. However, these materials contain non-abundant and/or toxic elements.[3–7] Silicon thin-film solar cells have been studied extensively;[8–13] but with this material, it is not easy to attain a high η as large as 20%. Thus, exploring alternative materials for thin-film solar cells is very important. Among such materials, we have been studying semiconducting barium disilicide (BaSi$_2$),[14] which consists of the safe and earth-abundant elements, Ba and Si, and possesses a bandgap of 1.3 eV that is appropriate for a single-junction solar cell.[15] In addition, BaSi$_2$ has a large absorption coefficient of 3×10^4 cm^{-1} at 1.5 eV, which is more than 40 times larger than that of c-Si.[15–18] In addition, undoped BaSi$_2$ exhibits a large minority-carrier diffusion length of 10 μm and a large minority-carrier lifetime of 10 μs.[19–22] Both electron and hole concentrations can be controlled in a wide range up to the order of 10^{19} cm^{-3} by doping Sb and B, respectively.[23,24] Recently, we attained an η value approaching 10% in p-BaSi$_2$/n-Si heterojunction solar cells.[25–27] Other types of solar cells such as Schottky-type BaSi$_2$, BaSi$_2$ nanowires, BaSi$_2$/perovskite stacked layers, and back-contacted BaSi$_2$ have also been proposed.[28–31] To further improve the η of BaSi$_2$ solar cells and to achieve homojunction solar cells, it is important to fabricate high-quality BaSi$_2$ epitaxial films.

In past works, we employed molecular beam epitaxy (MBE) to co-deposit Ba and Si on heated Si(111) substrates for the BaSi$_2$ growth.[32,33] Because the vapor pressure of Ba is much higher than that of Si, we grew these BaSi$_2$ films under a Ba-rich condition where, for example, the ratio of the Ba deposition rate to the Si deposition rate (R_{Ba}/R_{Si}) was fixed at 3.0.[33] These BaSi$_2$ films exhibit an n-type conductivity with an electron concentration n in the range from 5×10^{15} to 2×10^{16} cm^{-3}.[34–36] Regarding GaAs MBE growth, the density of the electron trap states located 0.82 eV from the conduction band edge increases with the As/Ga flux ratio.[37] This is because the Ga vacancies, As antisites, and interstitial As in the GaAs films work as electron traps. Therefore, we anticipate that the value of R_{Ba}/R_{Si} will have a huge impact on the characteristics of BaSi$_2$ films in the same way as the As/Ga flux ratio does. According to Kumar *et al.*,[38] the supercell approach based on first-principles density functional theory (DFT) revealed that the formation energies of point defects in BaSi$_2$ such as Si vacancies (V$_{Si}$), Ba antisites (Ba$_{Si}$), and interstitial Si (Si$_i$) are dependent upon the growth conditions. Hence, the amount of point defects and their species in BaSi$_2$ may change with R_{Ba}/R_{Si}. The purpose of this research is to fabricate undoped BaSi$_2$ epitaxial films with various values of R_{Ba}/R_{Si} and to examine the influence of R_{Ba}/R_{Si} on the crystalline qualities and the electrical and optical properties. Kumar *et al.* also found out that Si vacancies are most likely to occur in BaSi$_2$.[38] Thus, we also aim to reveal the influence of Si vacancies on the density of states (DOS) and total energies in the orthorhombic unit cell of BaSi$_2$.

II. METHODS

A. Formation of BaSi$_2$ films and characterizations

An ion-pumped MBE system (R-DEC) with a base pressure better than 10^{-8} Pa and equipped with a Knudsen cell for Ba and an electron-beam evaporation source for Si was used for sample preparation. The values of R_{Ba} and R_{Si} were controlled using an electron impact emission spectroscopy (EIES, INFICON) feedback system. We used low-resistivity n-Si(111) (resistivity $\rho = 0.01$ Ω cm) substrates for the photoresponsivity

measurement to make the contribution of photogenerated carriers in the Si substrate to the internal quantum efficiency (*IQE*) negligibly small. In contrast, we employed high-resistivity p-Si(111) ($\rho = 1000$–$10\,000\,\Omega\,\text{cm}$) for the Hall measurement, assuming that the undoped $BaSi_2$ exhibits n-type conductivity. Before growth, substrates were first cleaned according to standard RCA (Radio Corporation of America) procedure, followed by thermal cleaning at $900\,^\circ\text{C}$ for 30 min in the ultra-high vacuum chamber to remove a protective oxide layer on the surface. We then deposited Ba on a Si substrate heated at $500\,^\circ\text{C}$ by reactive deposition epitaxy to form a 3-nm-thick $BaSi_2$ template layer.[39] This template functions as a seed crystal source for the subsequent layer. Next, we grew 0.5-μm-thick undoped $BaSi_2$ on the templates at $580\,^\circ\text{C}$ by MBE. During the MBE growth, the R_{Si} was fixed at 0.9 nm/min and the R_{Ba} was varied from 0.9 to 4.6 nm/min, meaning that the $R_{\text{Ba}}/R_{\text{Si}}$ varied from 1.0 to 5.1. We then formed a 3-nm-thick amorphous Si at $180\,^\circ\text{C}$, which acts as a surface passivation layer for assuring a good electrical contact.[22,27,40] Finally, 80-nm-thick indium-tin-oxide (ITO) electrodes with 1 mm diameter were sputtered on the front surface and 150-nm-thick Al electrodes on the back surface of the Si substrate for the optical property evaluation. As described later, the *IQE* reached a maximum at $R_{\text{Ba}}/R_{\text{Si}} = 2.2$. To check the *IQE* spectra, we also grew one sample possessing an undoped $BaSi_2$ absorber as thick as $1.0\,\mu$m, with which the photocurrent density (J_L) beyond $40\,\text{mA/cm}^2$ was simulated in a $BaSi_2$ solar cell in Ref. 30.

The crystalline qualities of grown films were characterized by reflection high-energy electron diffraction (RHEED) along the Si[11$\bar{2}$] azimuth, and with x-ray diffraction (XRD; RIGAKU Smart Lab) using Cu Kα radiation, where Ge(220) single crystals were used to make the x-ray monochromatic. We measured θ-2θ XRD patterns to confirm the *a*-axis orientation of $BaSi_2$. We also conducted ω-scan x-ray rocking curve measurement to obtain full width at half maximum (FWHM) of a $BaSi_2(600)$ diffraction intensity to represent its crystalline quality. The actual atomic ratio of Ba to Si, $N_{\text{Ba}}/N_{\text{Si}}$, of the films was measured by Rutherford backscattering (RBS) spectrometry, where the incident He ion energy was set at 1.6 MeV and the backscattered ions with a scattering angle of 150° were detected. Photoresponse and reflectance spectra were evaluated at room temperature using a lock-in technique with a xenon lamp and a 25-cm-focal-length single monochromator (Bunko Keiki SM-1700A and RU-60N). The light intensity was calibrated using a pyroelectric sensor (Melles Griot 13PEM001/J). The carrier concentration of $BaSi_2$ was measured by Hall measurements using the van der Pauw method with an applied magnetic field of 0.8 T. We also measured the capacitance versus voltage (*C-V*) characteristics to estimate the carrier concentration in $BaSi_2$[35,36] at the condition when the carrier concentration decreased down to the order of $10^{15}\,\text{cm}^{-3}$, and hence, the carriers flowing through the Si substrate was not negligible in the Hall measurement. For this purpose, we fabricated 0.5-μm-thick undoped $BaSi_2$ on medium-doped p-Si(111) ($\rho = 0.1\,\Omega\,\text{cm}$). The hole concentration *p* of this substrate was $2 \times 10^{17}\,\text{cm}^{-3}$.

B. Computational details

The crystal structure of orthorhombic $BaSi_2$ is shown in Fig. 1. The stoichiometric description of the unit cell is Ba_8Si_{16}. In each $BaSi_2$ unit cell, there are two crystallographically inequivalent sites for Ba ($Ba^{(1)}$ and $Ba^{(2)}$) and three inequivalent sites for Si ($Si^{(3)}$, $Si^{(4)}$, and $Si^{(5)}$). Therefore, the atoms are distributed over $4Ba^{(1)}$, $4Ba^{(2)}$, $4Si^{(3)}$, $4Si^{(4)}$, and $8Si^{(5)}$. Total energies of $BaSi_2$ with three kinds of V_{Si} and DOSs were calculated using the Vienna *ab initio* simulation package code[41] based on DFT with the projector-augmented wave pseudopotential[42] and Perdew-Wang generalized gradient approximation method.[43] Total energy minimization was obtained via optimization of the lattice parameters and relaxation of the atomic positions in a conjugate gradient routine. Using an energy cutoff of 600 eV and a $6 \times 8 \times 4$ grid of Monkhorst–Pack points, the convergence in the total energy was better than 1 meV/atom.[44] Hereafter, we describe $BaSi_2$ with one V_{Si} as $Ba_8Si_{15}V_{\text{Si}(3)}$, in which one of the four $Si^{(3)}$ sites is vacant, $Ba_8Si_{15}V_{\text{Si}(4)}$, in which one of the four $Si^{(4)}$ sites is missing, or $Ba_8Si_{15}V_{\text{Si}(5)}$, in which one of the eight $Si^{(5)}$ sites is vacant. The calculated total energies of these compounds are summarized in Table I. In our framework of first-principles calculations, we cannot take into account thermal effects at the finite temperature to the DFT calculation.

III. RESULTS AND DISCUSSION

A. Experimental results

Figure 2 shows the RHEED patterns observed along the Si[11$\bar{2}$] azimuth and the θ-2θ XRD patterns for $BaSi_2$ films formed with different values of $R_{\text{Ba}}/R_{\text{Si}}$. As shown in Fig. 2, sharp streaky RHEED patterns and intense *a*-axis-oriented diffraction peaks in the XRD patterns can be observed.
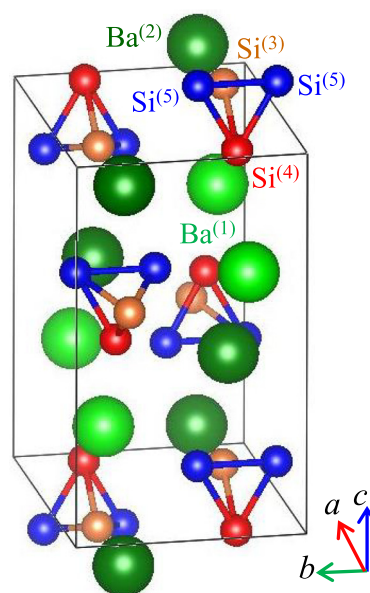

FIG. 1. Crystal structure of $BaSi_2$. There are two crystallographically inequivalent sites for Ba ($Ba^{(1)}$ and $Ba^{(2)}$) and three inequivalent sites for Si ($Si^{(3)}$, $Si^{(4)}$, and $Si^{(5)}$) in the orthorhombic unit cell of $BaSi_2$.

TABLE I. Calculated electronic energies for Ba_8Si_{16}, $Ba_8Si_{15}V_{Si(3)}$, $Ba_8Si_{15}V_{Si(4)}$, and $Ba_8Si_{15}V_{Si(5)}$.

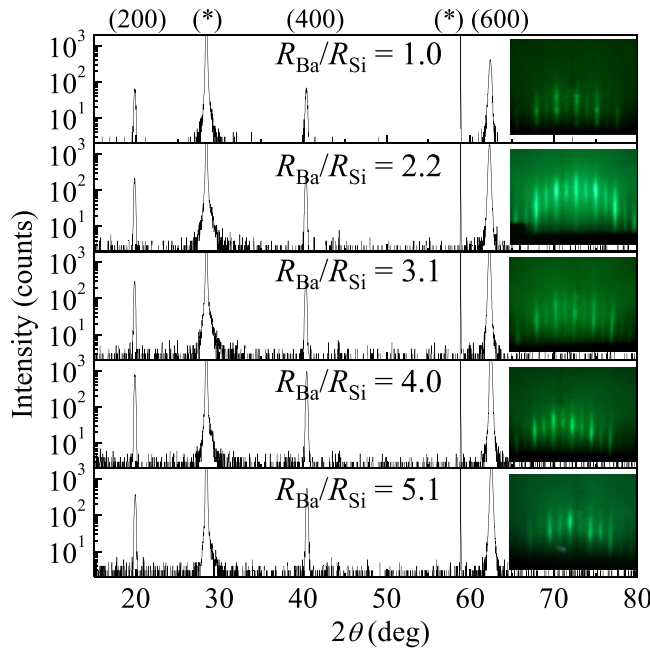| Compound	Total energy (eV)
$8Ba + 16Si \rightarrow Ba_8Si_{16}$	-133.696
$Ba_8Si_{16} \rightarrow Ba_8Si_{15}V_{Si(3)} + Si$	-132.591 (-127.174–5.417)
$Ba_8Si_{16} \rightarrow Ba_8Si_{15}V_{Si(4)} + Si$	-132.519 (-127.102–5.417)
$Ba_8Si_{16} \rightarrow Ba_8Si_{15}V_{Si(5)} + Si$	-132.455 (-127.038–5.417)

FIG. 2. θ-2θ XRD and RHEED patterns of $BaSi_2$ layers with various values of R_{Ba}/R_{Si}. The RHEED patterns were observed along the $Si[11\bar{2}]$ azimuth just after the growth of $BaSi_2$. The asterisk (*) indicates the diffraction of the substrate used.

These results show that a-axis-oriented $BaSi_2$ epitaxial films were grown on the Si(111) substrate, regardless of the R_{Ba}/R_{Si}.

Figure 3 presents the R_{Ba}/R_{Si} dependences of $BaSi_2$ growth rate and FWHM values obtained from an ω-scan x-ray rocking curve using a $BaSi_2(600)$ diffraction intensity. The $BaSi_2$ growth rate monotonically increases as the R_{Ba} increases. The FWHM value decreases with increasing R_{Ba}/R_{Si}
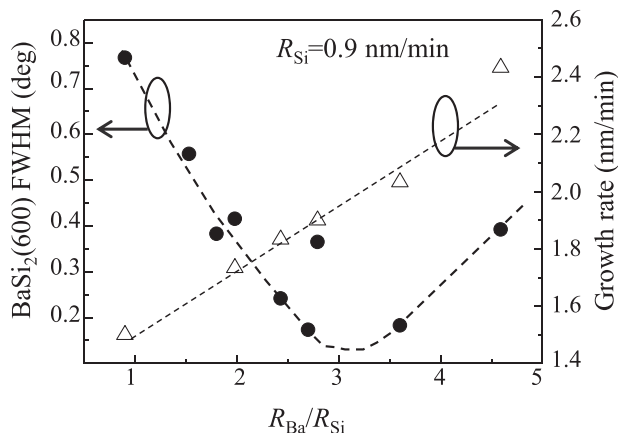

FIG. 3. Dependences of FWHM of $BaSi_2(600)$ intensity and $BaSi_2$ growth rate on R_{Ba}/R_{Si}.

and reaches a minimum at $R_{Ba}/R_{Si} \sim 3$, and increases with R_{Ba}/R_{Si}. This result suggests that the R_{Ba}/R_{Si} should be around 3 from the view point of crystalline quality of $BaSi_2$. That is why we have chosen the R_{Ba}/R_{Si} value at 3.0 for the MBE growth of $BaSi_2$ films.[33]

Figure 4(a) shows the RBS spectra and Fig. 4(b) presents the resultant N_{Ba}/N_{Si} depth profiles for $BaSi_2$ films with $R_{Ba}/R_{Si} = 1.0$, 2.2, and 4.0. The $N_{Ba}/N_{Si} > 0.5$ means that Ba was in excess of stoichiometric conditions, while $N_{Ba}/N_{Si} < 0.5$ indicates that the Ba amount was deficient. The N_{Ba}/N_{Si} value in the sample with $R_{Ba}/R_{Si} = 4.0$ was greater than that with $R_{Ba}/R_{Si} = 2.2$ along the entire depth. Similarly, the N_{Ba}/N_{Si} value in the sample with $R_{Ba}/R_{Si} = 2.2$ was greater than that with $R_{Ba}/R_{Si} = 1.0$. Thus, we assume that the amount of point defects and their species in $BaSi_2$ of these three samples are different. In addition, the N_{Ba}/N_{Si} decreased when it approached the $BaSi_2$/Si interface for all the samples even though they were grown under a constant value of R_{Ba}/R_{Si} during the growth. This result suggests that the Si substrate supplied Si atoms to the $BaSi_2$ layer during the MBE growth.

The photoresponse spectra of the samples are shown in Fig. 5(a). A bias voltage $V_{bias} = -1$ V was applied to the front-surface ITO electrode with respect to the back-surface Al electrode to extract the photogenerated holes in the $BaSi_2$
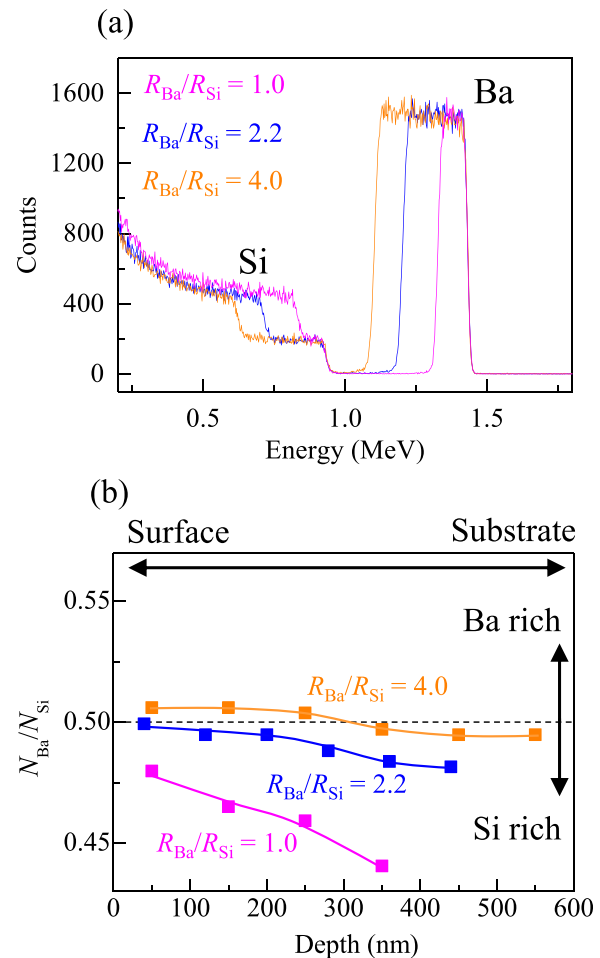

FIG. 4. (a) RBS spectra for $BaSi_2$ with $R_{Ba}/R_{Si} = 1.0$, 2.2 and 4.0, and (b) depth profiles of the Ba/Si atomic ratio, N_{Ba}/N_{Si}.
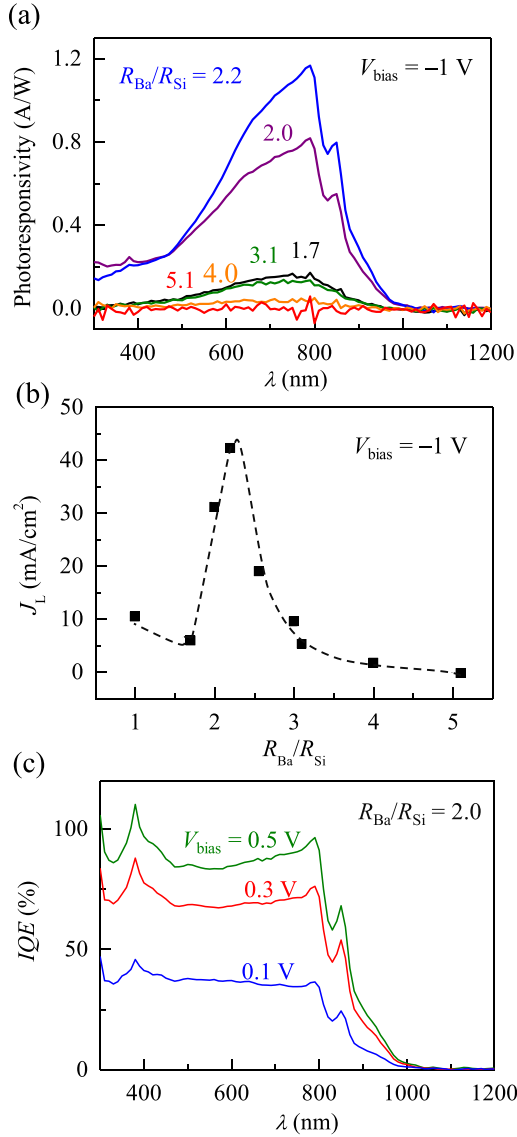
(a)

(b)

(c)

FIG. 5. (a) Photoresponse spectra of 0.5-μm-thick $BaSi_2$ grown with various R_{Ba}/R_{Si} values measured under a bias voltage of -1 V applied to the front ITO electrode with respect to the back Al electrode, (b) dependence of photocurrent density J_L on R_{Ba}/R_{Si}, and (c) bias voltage dependence of *IQE* spectra of 1.0-μm-thick $BaSi_2$ with $R_{Ba}/R_{Si} = 2.0$ grown on p-$BaSi_2$(50 nm)/ p-Si(111) ($\rho < 0.01\ \Omega$ cm).

film. To our surprise, the photoresponse spectra were quite sensitive to variations in R_{Ba}/R_{Si}. To clarify the impact of the spectral response, we converted them to the values of *IQE* and subsequently to the photocurrent density J_L using

$$J_L = q \int \Phi_{AM1.5G} \times IQE\ dE, \tag{1}$$

where q is the elemental charge and $\Phi_{AM1.5G}$ is the photon flux density of AM1.5G. As shown in Fig. 5(b), the J_L reached a maximum at $R_{Ba}/R_{Si} = 2.2$. Figure 5(c) shows the *IQE* spectra of the 1.0-μm-thick $BaSi_2$ film grown with $R_{Ba}/R_{Si} = 2.0$ at $V_{bias} = 0.1$, 0.3, and 0.5 V. For this sample, we chose the R_{Ba}/R_{Si} value at 2.0 instead of 2.2. This is because the N_{Ba}/N_{Si} may exceed 0.5 in the region close to the surface for $R_{Ba}/R_{Si} = 2.2$ when the $BaSi_2$ thickness increases from 500 nm to 1 μm, leading to the degradation of the photoresponse

properties. The *IQE* exceeds 80% in a wide wavelength range at $V_{bais} = 0.5$ V, demonstrating the great potential of $BaSi_2$ homojunction solar cells. In the present work, the photogenerated carriers in $BaSi_2$, where the electric field exists because of V_{bias}, are collected by drifting. The *IQE* is proportional to the ratio of the carrier lifetime to the carrier transit time. With increasing V_{bias}, the drift velocity of carriers increases, leading to a decrease in the carrier transit time. Therefore, more holes and electrons can reach the ITO electrode and the n-Si region before recombination, respectively. When the transit time becomes much shorter than the carrier lifetime, the *IQE* may exceed 100% as shown in the case of $V_{bias} = 0.5$ V. This phenomenon has been applied to practical devices such as photoconductors.

We next measured the carrier concentration of each sample and examined the correlation between the photoresponsivity and the carrier concentration. Figure 6(a) shows the relationship between R_{Ba}/R_{Si} and carrier concentration as evaluated by Hall measurements and/or *C-V* measurements. For this purpose, we have fabricated eight samples with $R_{Ba}/R_{Si} = 1.0$, 1.7, 2.0, 2.2, 2.6, 3.0, 3.5, and 4.0. Among them, the carrier type of the $BaSi_2$ films grown with $R_{Ba}/R_{Si} = 2.0$, 2.2, and 2.6 was *p*. Other samples showed n-type conductivity, and the electron concentration increases for both increasing and decreasing R_{Ba}/R_{Si} values. The hole concentration reached a minimum of approximately $1 \times 10^{15}\ cm^{-3}$ at $R_{Ba}/R_{Si} = 2.2$. This small majority carrier concentration may reduce the carrier recombination of photogenerated minority
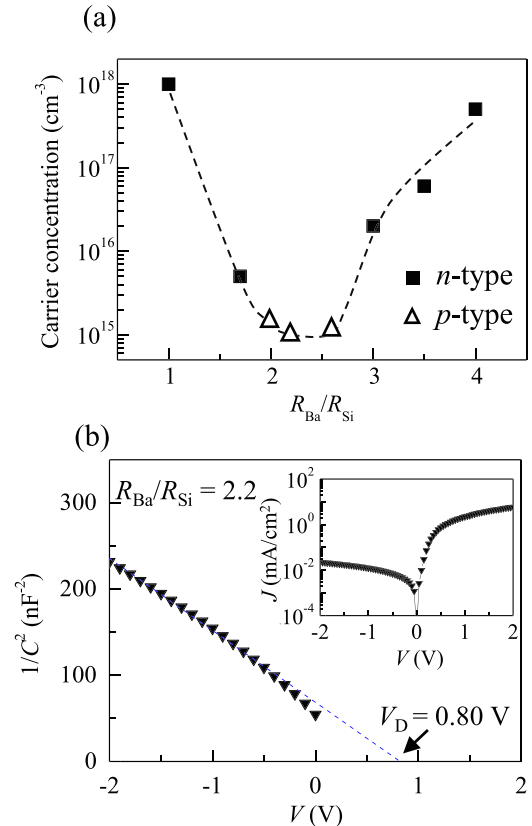
(a)

(b)

FIG. 6. (a) Relationship between the carrier concentration and R_{Ba}/R_{Si}. (b) Capacitance ($1/C^2$) versus voltage (V) plot of a $BaSi_2$/p-Si heterojunction diode with $R_{Ba}/R_{Si} = 2.2$. The current density versus voltage plot is inserted.

carriers (electrons) with majority carriers (holes) and hence leads to an enhanced minority-carrier lifetime and, consequently, gives rise to large spectral response and J_L, as shown in Figs. 5(a) and 5(b). Regarding the BaSi$_2$ film with R_{Ba}/R_{Si} = 2.0–2.6, we estimated the carrier concentration by the C-V method because the carrier concentration decreased so much. Figure 6(b) shows an example of the $1/C^2$ versus V plot for the sample with R_{Ba}/R_{Si} = 2.2. The current density versus voltage plot is also shown. The current density increased when the negative bias voltage was applied to the ITO electrode with respect to the p-Si substrate. The carrier type by the Hall measurement was found to be holes. The built-in voltage V_D was approximately 0.80 V, and this value corresponds to the difference in the Fermi level between BaSi$_2$ ($E_F^{BaSi_2}$) and Si (E_F^{Si}) before contact. In our previous report,[35,36] the V_D value was 1.5 V for n-BaSi$_2$ ($n = 2 \times 10^{16}$ cm^{-3}) formed with R_{Ba}/R_{Si} = 3.0 on the same p-Si substrate ($p = 2 \times 10^{17}$ cm^{-3}). Here, we evaluate the position of $E_F^{BaSi_2}$ for BaSi$_2$ with R_{Ba}/R_{Si} = 2.2. The electron affinity of BaSi$_2$ and Si is $q\chi_{BaSi_2}$ = 3.2 eV (Ref. 45) and $q\chi_{Si}$ = 4.05 eV, respectively, and their bandgaps are $E_g^{BaSi_2} = 1.3$ eV and $E_g^{Si} = 1.1$ eV. Thus, the valence band offset ΔE_V is given by $q\chi_{Si} + E_g^{Si} - (q\chi_{BaSi_2} + E_g^{BaSi_2}) = 0.65$ eV. Assuming that the effective density of states at the valence band of Si, N_V^{Si}, is 1.04×10^{19} cm^{-3}, the E_F^{Si} is located at $k_B T \ln(N_V^{Si}/p) = 0.10$ eV from the valence-band edge of Si, where k_B is the Boltzmann constant and T is the absolute temperature. Therefore, the $E_F^{BaSi_2}$ is positioned at around 0.25 eV ($= 0.80 + 0.10 - 0.65$) above the valence band edge of BaSi$_2$, $E_V^{BaSi_2}$, suggesting that the BaSi$_2$ exhibits p-type conductivity. Therefore, the hole concentration of the BaSi$_2$ film with R_{Ba}/R_{Si} = 2.2 is thus estimated to be approximately 1×10^{15} cm^{-3} using

$$p = N_V^{BaSi_2} \exp\left(-\frac{E_F^{BaSi_2} - E_V^{BaSi_2}}{k_B T}\right). \qquad (2)$$

Here, the effective density of states at the valence band of BaSi$_2$, $N_V^{BaSi_2}$, is approximately 2.0×10^{19} cm^{-3} from the principle-axis components of the effective mass tensor for holes and two equivalent valleys at $E_V^{BaSi_2}$.[16] The obtained hole concentration is also explained by the slope of the $1/C^2$ versus V plot. According to Kumar *et al.*,[38] V$_{Si}$, Ba$_{Si}$, and Si$_i$ are predominant defects in BaSi$_2$. We expect that these point defects form during the MBE growth when the R_{Ba}/R_{Si} is deviated from the ideal value and that they work as donor impurities. The conduction type changed from n-type to p-type in the BaSi$_2$ films grown with R_{Ba}/R_{Si} = 2.0–2.6 when the density of Si vacancies which act as donors became smaller than the residual hole concentration, likely owing to B atoms. This is because the optimum value of R_{Ba}/R_{Si} minimizes Si vacancies. It is reported that p-type doping due to B contamination is routinely detected in Si MBE when using standard MBE cleaning schemes.[46,47] The influence of the wet chemical precleaning as well as of the *in situ* thermal cleaning in the ultra-high vacuum was investigated with respect to this effect.[46] We cannot detect such a small B concentration of the order of 10^{15} cm^{-3} by secondary ion mass spectrometry (SIMS), which is much smaller than the SIMS detection limit of B in BaSi$_2$.

B. Calculation results

To elucidate what happens in Ba$_8$Si$_{15}$V$_{Si(3)}$, Ba$_8$Si$_{15}$V$_{Si(4)}$, and Ba$_8$Si$_{15}$V$_{Si(5)}$, we discuss here their total DOSs and energies. The binding energy of Ba$_8$Si$_{16}$ was calculated to be -133.696 eV. The total energy of Ba$_8$Si$_{15}$V$_{Si(3)}$, for example, is calculated to be $(-127.174) + (-5.417) = -132.591$ eV. In the same way, the total energies of Ba$_8$Si$_{15}$V$_{Si(4)}$ and Ba$_8$Si$_{15}$V$_{Si(5)}$ were calculated as summarized in Table I. From an energetic point of view, Ba$_8$Si$_{15}$V$_{Si(3)}$ is most likely to form, implying that the V$_{Si}$ is most likely to be located at the Si$^{(3)}$ sites. It should be noted that Ba$_8$Si$_{15}$V$_{Si(4)}$ is also energetically favorable because of a small energy difference between Ba$_8$Si$_{15}$V$_{Si(3)}$ and Ba$_8$Si$_{15}$V$_{Si(4)}$. Figure 7 shows the total DOSs of (a) Ba$_8$Si$_{16}$, (b) Ba$_8$Si$_{15}$V$_{Si(3)}$, (c) Ba$_8$Si$_{15}$V$_{Si(4)}$, and (d) Ba$_8$Si$_{15}$V$_{Si(5)}$ near the Fermi level, E_F. The energy zero of the DOS curve is taken at their E_F. There are localized states within the bandgap as shown in Figs. 7(b)–7(d). These results suggest that the deviation from stoichiometry promotes recombination
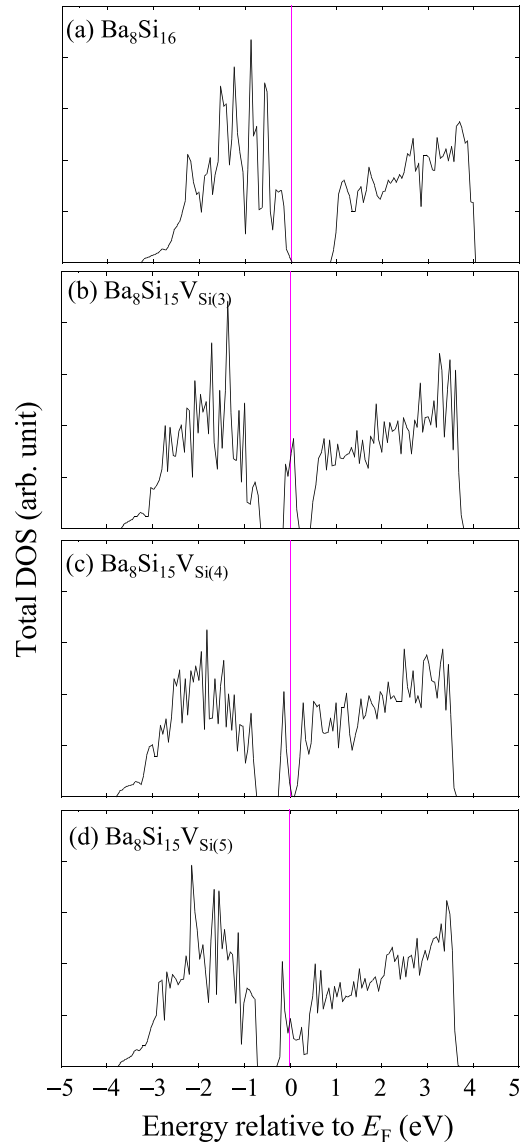

FIG. 7. Total DOSs of (a) Ba$_8$Si$_{16}$, (b) Ba$_8$Si$_{15}$V$_{Si(3)}$, (c) Ba$_8$Si$_{15}$V$_{Si(4)}$, and (d) Ba$_8$Si$_{15}$V$_{Si(5)}$. Color line shows the position of E_F.

of electron-hole pairs via localized states and therefore leads to the degradation in *IQE*. In Fig. 7(c), the E_F is positioned closer to the conduction band edge, suggesting that $Ba_8Si_{15}V_{Si(4)}$ is an n-type semiconductor. We speculate that that is why the electron concentration increased in Fig. 6(a) with R_{Ba}/R_{Si} being away from the optimum value of around 2.2. The present calculation results show that it is very important to satisfy stoichiometry in a $BaSi_2$ absorber by controlling R_{Ba}/R_{Si} precisely. This is, however, not consistent with the fact that the $BaSi_2$ film with $R_{Ba}/R_{Si} = 2.2$ ($N_{Ba}/N_{Si} < 0.5$) was optimum as shown in Fig. 4(b). We think that excess Si atoms are precipitated in the form of Si microcrystallites as discussed below. Figure 8 shows the Raman spectrum of a 0.5-μm-thick *a*-axis-oriented $BaSi_2$ epitaxial film grown with $R_{Ba}/R_{Si} = 2.0$, measured at room temperature by NRS-5100 (RIGAKU Smart Lab) using a frequency doubled Nd:YAG laser (532 nm). The Raman lines originate from Si tetrahedra with T_h symmetry in the lattice of $BaSi_2$. The transverse optical phonon line of Si (Si_{TO}) was observed even in such a thick $BaSi_2$ film. Considering that the absorption coefficient of $BaSi_2$ at this wavelength is $\alpha = 3 \times 10^5 \, cm^{-1}$,[15] and hence the penetration depth of the laser light was limited to around $1/\alpha \times 3 \sim 0.1 \, \mu$m, the Si_{TO} signal is considered to originate from Si precipitates in the $BaSi_2$ film. Similar Si_{TO} signals were detected in $BaSi_2$ (Ref. 48) and β-$FeSi_2$ films[49] by Raman spectroscopy, and they were ascribed to the Si precipitates in the films.

IV. SUMMARY

We fabricated 0.5-μm-thick undoped $BaSi_2$ epitaxial films on Si(111) substrates with various values of R_{Ba}/R_{Si} ranging from 1.0 to 5.1 and characterized their electrical and optical properties. The RBS measurement revealed that the N_{Ba}/N_{Si} value decreased close to the $BaSi_2$/Si interface. This was attributed to the Si atoms diffused from the Si substrate during the MBE growth. The photoresponsivity drastically changed as the R_{Ba}/R_{Si} was varied, and the J_L reached a maximum at $R_{Ba}/R_{Si} = 2.2$. As a result of the Hall and *C-V* measurements, it was found that the electron concentration decreased when R_{Ba}/R_{Si} approached the optimum value, and the $BaSi_2$ films grown with $R_{Ba}/R_{Si} = 2.0$, 2.2, and 2.6 exhibited p-type conductivity. The lowest hole concentration of approximately $1 \times 10^{15} \, cm^{-3}$ ever reported was obtained at
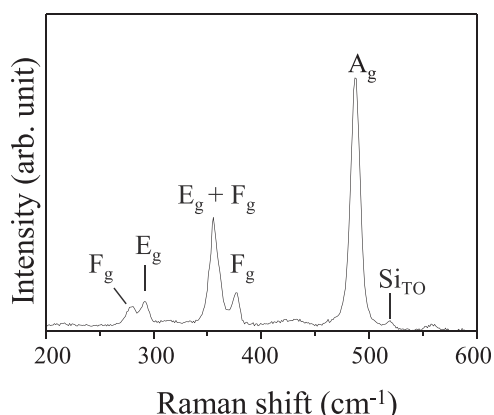
$R_{Ba}/R_{Si} = 2.2$. First-principles calculations by VASP predicted that $BaSi_2$ containing Si vacancies induce localized states within the bandgap. Therefore, it is very important to control R_{Ba}/R_{Si} precisely to improve the $BaSi_2$ solar cell performance because various disorders or defects are sensitive to R_{Ba}/R_{Si}.

FIG. 8. Raman spectrum of a 0.5-μm-thick $BaSi_2$ epitaxial film with $R_{Ba}/R_{Si} = 2.0$ at RT.

[1]K. Yoshikawa, H. Kawasaki, W. Yoshida, T. Irie, K. Konishi, K. Nakano, T. Uto, D. Adachi, M. Kanematsu, H. Uzu, and K. Yamamoto, Nat. Energy **2**, 17032 (2017).
[2]K. Masuko, M. Shigematsu, T. Hashiguchi, D. Fujishima, M. Kai, N. Yoshimura, T. Yamaguchi, Y. Ichihashi, T. Mishima, N. Matsubara, T. Yamanishi, T. Takahama, M. Taguchi, E. Maruyama, and S. Okamoto, IEEE J. Photovoltaics **4**, 1433 (2014).
[3]P. Jackson, D. Hariskos, R. Wuerz, O. Kiowski, A. Bauer, T. M. Friedlmeier, and M. Powalla, Phys. Status Solidi RRL **9**, 28 (2015).
[4]P. Jackson, R. Wuerz, D. Hariskos, E. Lotter, W. Witte, and M. Powalla, Phys. Status Solidi RRL **10**, 583 (2016).
[5]X. Wu, Sol. Energy **77**, 803 (2004).
[6]J. Burschka, N. Pellet, S.-J. Moon, R. Humphry-Baker, P. Gao, M. K. Nazeeruddin, and M. Grätzel, Nature **499**, 316 (2013).
[7]W. S. Yang, J. H. Noh, N. J. Jeon, Y. C. Kim, S. Ryu, J. Seo, and S. I. Seok, Science **348**, 1234 (2015).
[8]H. Sai, T. Matsui, T. Koida, K. Matsubara, M. Kondo, S. Sugiyama, H. Katayama, Y. Takeuchi, and I. Yoshida, Appl. Phys. Lett. **106**, 213902 (2015).
[9]C. Trompoukis, I. Abdo, R. Cariou, I. Cosme, W. Chen, O. Deparis, A. Dmitriev, E. Drouard, M. Foldyna, E. G. Caurel, I. Gordon, B. Heidari, A. Herman, L. Lalouat, K. D. Lee, J. Liu, K. Lodewijks, F. Mandorlo, I. Massiot, A. Mayer, V. Mijkovic, J. Muller, R. Orobtchouk, G. Poulain, P. Prod'Homme, P. R. Cabarrocas, C. Seassal, J. Poortmans, R. Mertens, O. E. Daif, and V. Depauw, Phys. Status Solidi A **212**, 140 (2015).
[10]H. Tan, E. Moulin, F. T. Si, J. W. Schüttauf, M. Stuckelberger, O. Isabella, F. J. Haug, C. Ballif, M. Zeman, and A. H. M. Smets, Prog. Photovoltaics **23**, 949 (2015).
[11]H. Sai, T. Matsui, K. Saito, M. Kondo, and I. Yoshida, Prog. Photovoltaics **23**, 1572 (2015).
[12]F. Meillaud, M. Boccard, G. Bugnon, M. Despeisse, S. Hänni, F.-J. Haug, J. Persoz, J.-W. Schüttauf, M. Stuckelberger, and C. Ballif, Mater. Today **18**, 378 (2015).
[13]M. Konagai, Jpn. J. Appl. Phys., Part 1 **50**, 030001 (2011).
[14]T. Suemasu and N. Usami, J. Phys. D: Appl. Phys. **50**, 023001 (2017).
[15]K. Toh, T. Saito, and T. Suemasu, Jpn. J. Appl. Phys., Part 1 **50**, 068001 (2011).
[16]D. B. Migas, V. L. Shaposhnikov, and V. E. Borisenko, Phys. Status Solidi B **244**, 2611 (2007).
[17]M. Kumar, N. Umezawa, and M. Imai, J. Appl. Phys. **115**, 203718 (2014).
[18]M. Kumar, N. Umezawa, and M. Imai, Appl. Phys. Express **7**, 071203 (2014).
[19]M. Baba, K. Toh, K. Toko, N. Saito, N. Yoshizawa, K. Jiptner, T. Sakiguchi, K. O. Hara, N. Usami, and T. Suemasu, J. Cryst. Growth **348**, 75 (2012).
[20]K. O. Hara, N. Usami, K. Toh, M. Baba, K. Toko, and T. Suemasu, J. Appl. Phys. **112**, 083108 (2012).
[21]K. O. Hara, N. Usami, K. Nakamura, R. Takabe, M. Baba, K. Toko, and T. Suemasu, Appl. Phys. Express **6**, 112302 (2013).
[22]R. Takabe, K. O. Hara, M. Baba, W. Du, N. Shimada, K. Toko, N. Usami, and T. Suemasu, J. Appl. Phys. **115**, 193510 (2014).

[23]M. A. Khan, K. O. Hara, W. Du, M. Baba, K. Nakamura, M. Suzuno, K. Toko, N. Usami, and T. Suemasu, Appl. Phys. Lett. **102**, 112107 (2013).

[24]M. Kobayashi, Y. Matsumoto, Y. Ichikawa, D. Tsukada, and T. Suemasu, Appl. Phys. Express **1**, 051403 (2008).

[25]D. Tsukahara, S. Yachi, H. Takeuchi, R. Takabe, W. Du, M. Baba, Y. Li, K. Toko, N. Usami, and T. Suemasu, Appl. Phys. Lett. **108**, 152101 (2016).

[26]S. Yachi, R. Takabe, K. Toko, and T. Suemasu, Appl. Phys. Lett. **109**, 072103 (2016).

[27]R. Takabe, S. Yachi, W. Du, D. Tsukahara, H. Takeuchi, K. Toko, and T. Suemasu, AIP Adv. **6**, 085107 (2016).

[28]A. Sasaki, Y. Kataoka, K. Aoki, S. Saito, K. Kobayashi, T. Ito, K. Kakushima, and H. Iwai, Jpn. J. Appl. Phys., Part 1 **54**, 031202 (2015).

[29]A. Pokhrel, L. Samad, F. Meng, and S. Jin, Nanoscale **7**, 17450 (2015).

[30]R. Vismara, O. Isabella, and M. Zeman, Proc. SPIE **9898**, 98980J (2016).

[31]R. Vismara, O. Isabella, and M. Zeman, Opt. Express **25**, A402 (2017).

[32]Y. Inomata, T. Nakamura, T. Suemasu, and F. Hasegawa, Jpn. J. Appl. Phys., Part 2 **43**, L478 (2004).

[33]R. Takabe, K. Nakamura, M. Baba, W. Du, M. A. Khan, K. Toko, M. Sasase, K. O. Hara, N. Usami, and T. Suemasu, Jpn. J. Appl. Phys., Part 1 **53**, 04ER04 (2014).

[34]K. Morita, Y. Inomata, and T. Suemasu, Thin Solid Films **508**, 363 (2006).

[35]H. Takeuchi, W. Du, M. Baba, R. Takabe, K. Toko, and T. Suemasu, Jpn. J. Appl. Phys., Part 1 **54**, 07JE01 (2015).

[36]W. Du, M. Baba, K. Toko, K. O. Hara, K. Watanabe, T. Sekiguchi, N. Usami, and T. Suemasu, J. Appl. Phys. **115**, 223701 (2014).

[37]P. K. Bhattacharya, J. W. Ku, S. J. T. Owen, V. Aebi, C. B. Cooper III, and R. L. Moon, Appl. Phys. Lett. **36**, 304 (1980).

[38]M. Kumar, N. Umezawa, W. Zou, and M. Imai, J. Mater. Chem. A **5**, 25293 (2017).

[39]Y. Inomata, T. Nakamura, T. Suemasu, and F. Hasegawa, Jpn. J. Appl. Phys., Part 1 **43**, 4155 (2004).

[40]R. Takabe, H. Takeuchi, W. Du, K. Ito, K. Toko, S. Ueda, A. Kimura, and T. Suemasu, J. Appl. Phys. **119**, 165304 (2016).

[41]G. Kresse and D. Joubert, Phys. Rev. B **59**, 1758 (1999).

[42]P. E. Blöchl, Phys. Rev. B **50**, 17953 (1994).

[43]J. P. Perdew, J. A. Chevary, S. H. Vosko, K. A. Jackson, M. R. Pederson, D. J. Singh, and C. Fiolhais, Phys. Rev. B **46**, 6671 (1992).

[44]H. J. Monkhorst and J. D. Pack, Phys. Rev. B **13**, 5188 (1976).

[45]T. Suemasu, K. Morita, M. Kobayashi, M. Saida, and M. Sasaki, Jpn. J. Appl. Phys., Part 2 **45**, L519 (2006).

[46]A. Casel, E. Kasper, H. Kibbel, and E. Sasse, J. Vac. Sci. Technol. B **5**, 1650 (1987).

[47]K. Miki, K. Sakamoto, and T. Sakamoto, Surf. Sci. **406**, 312 (1998).

[48]Y. Terai, H. Yamaguchi, H. Tsukamoto, N. Murakoso, M. Iinuma, and T. Suemasu, Jpn. J. Appl. Phys., Part 1 **56**, 05DD02 (2017).

[49]M. Iinuma, H. Tsukamoto, N. Murakoso, H. Yamaguchi, and Y. Terai, JJAP Conf. Proc. **5**, 011106 (2017).